PERFORMANCE ANALYSIS OF NON-CONTACTING GAS FACE SEALS USING THE FINITE ELEMENT METHOD

Marco Túlio Corrêa de Faria
Universidade Federal de Minas Gerais, Av. Antônio Carlos, 6627 – Pampulha – Belo Horizonte - MG
mtcdf@uol.com.br

Raimundo Eduardo Cota
Gerdau Açominas, Rodovia MG 443, Km 7 - Fazenda do Cadete - Ouro Branco - MG
raimundo.cota@gerdau.com.br

Frederico Vaz de Mello
Universidade Federal de Minas Gerais, Av. Antônio Carlos, 6627 – Pampulha – Belo Horizonte - MG
fred_vazmello@yahoo.com.br

Abstract. *Enhancements on gas face seals performance have been acquired by introducing grooves or some form of geometric roughness onto the mating seal plates. Reducing fluid leakage through the seal surface has been the main motivation for the development of efficient sealing technology to industrial turbomachinery. Pressure dams are generally etched on the seal inner and outer radii to improve even more the seal capability of reducing the gas leakage to atmosphere. This paper presents a finite element analysis carried out to determine the opening force, the flow leakage and the dynamic force coefficients of flat gas face seals with pressure dams operating under stringent conditions. Several curves of steady-state and dynamic seal performance characteristics depict the influence of the pressure dam position and width on the seal performance and efficiency.*

Keywords*: Gas Seals, Face Seals, Non-contacting Seals, Pressure Dams, Stepped Seals*

1. INTRODUCTION

The search for more efficient and safer sealing systems for high-performance turbomachinery employed in the oil, petrochemical, chemical and general process industries has been the main motivation for the development of new techniques and procedures for mechanical seal analysis and design (Dulak, 1990; Allaire, 1984; Wasser, 1994). Current environmental regulations on hazardous fluid emissions in industrial plants have cut down the admissible levels of fluid leakage into the atmosphere, forcing the seal manufacturers to invest in new sealing technologies. Within all novel and efficient sealing technologies that have been recently used for seal design, the gas sealing technology deserves to be highlighted (Gabriel, 1994; Burgmann, 1997). The application of gas lubrication technology in end seals has permitted the development of zero emission noncontacting face seals for industrial pumps (Lebeck and Albor, 1999).

Gas lubricated face seals meet satisfactorily the requirements of low leakage rate, wear free operation and low power consumption for industrial compressors, pumps, agitators and other turbomachines (Burgmann, 1997). Grooves, pockets, steps and textured pores have been etched on either of the seal mating plates to improve the gas face seal performance (Etsion *et al.*, 1992; Kowalski and Basu, 1995; Salant and Homiller, 1992a; Basu, 1992). All these typical gas seal plate geometries possess an unprofiled area, the sealing dam, which can be located at either the seal inner or outer radius (Salant and Homiller, 1992b). This pressure dam is introduced into the seal face to reduce leakage and increase axial stiffness. The pressure dam location determines the seal radial flow direction. Outer dams are generally employed for outward radial flow within the seal plates and inner dams for inward radial flow.

Most of the studies performed on gas face seals deal with the analysis of the influence of the seal-mating plate patterns, which generally include various types of grooves, face waviness, radial taper and face texture, on the seal performance (Tournerie *et al.*,1994; Zirkelback and San Andrés, 1999; Hernandez and Boudet, 1995; Salant and Homiller, 1992b; Etsion *et al.*, 1998; Basu, 1992; Wasser, 1994). In the analyses of grooved face seals, the main concern has been the parametric study of the influence of the groove geometry, in conjunction with or without the sealing dam, on the seal behavior. The influence of the pressure dam geometry on the performance of gas face seals is still an important subject that has not been well exploited in the technical literature.

In order to bring some insights into the influence of the pressure dam geometry on the gas lubricated face seal behavior, this paper presents a finite element analysis of gas face seal with inner and outer pressure dams. The classical Reynolds equation for compressible fluids is the basis for the finite element (FEM) procedure developed in this work. A perturbation method is applied on the Reynolds equation to render the zero-th and first-order lubrication equations, which are employed to estimate some steady-state and dynamic seal performance characteristics. The FEM procedure is based on the Galerkin weighted residual method (Huebner *et al*., 1995). The gas flow through the seal is assumed axi-symmetric. In the analysis, the seal mating plates are made flat and smooth to allow the exclusive evaluation of the pressure dam geometric parameters on the seal performance. Seal performance characteristics, such as seal opening force, flow leakage, and frequency dependent stiffness and damping force coefficients, are computed in relation to some

seal parameters, such as dam extent, clearance ratio and seal width. The model validation is performed by comparing the finite element predictions with approximated analytical solutions for gas-lubricated flat mechanical face seals.

2. GAS FACE SEAL GEOMETRY AND BASIC GOVERNING EQUATION

To illustrate the basic geometric configuration of gas face seals, Figure 1 shows schematic drawings of the seal plate with pressure dam. On Fig. 1, the pressure dam heights are intentionally exaggerated. A schematic view of the geometry of a flat mechanical face seal with outer pressure dam is depicted on Fig 2. The sealing dam can be located at either the seal inner radius or outer radius, depending on the radial pressure ratio.

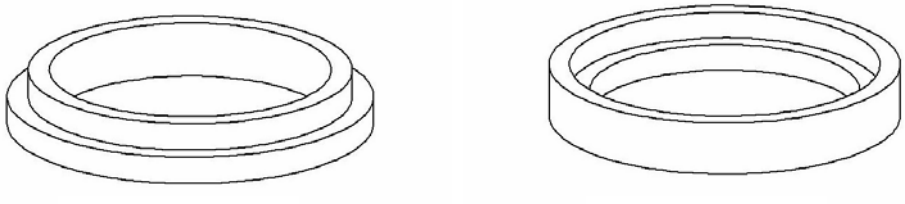

(a) Inner dam seal (b) Outer dam seal

Figure 1. Schematic drawings of seal plates with pressure dam.

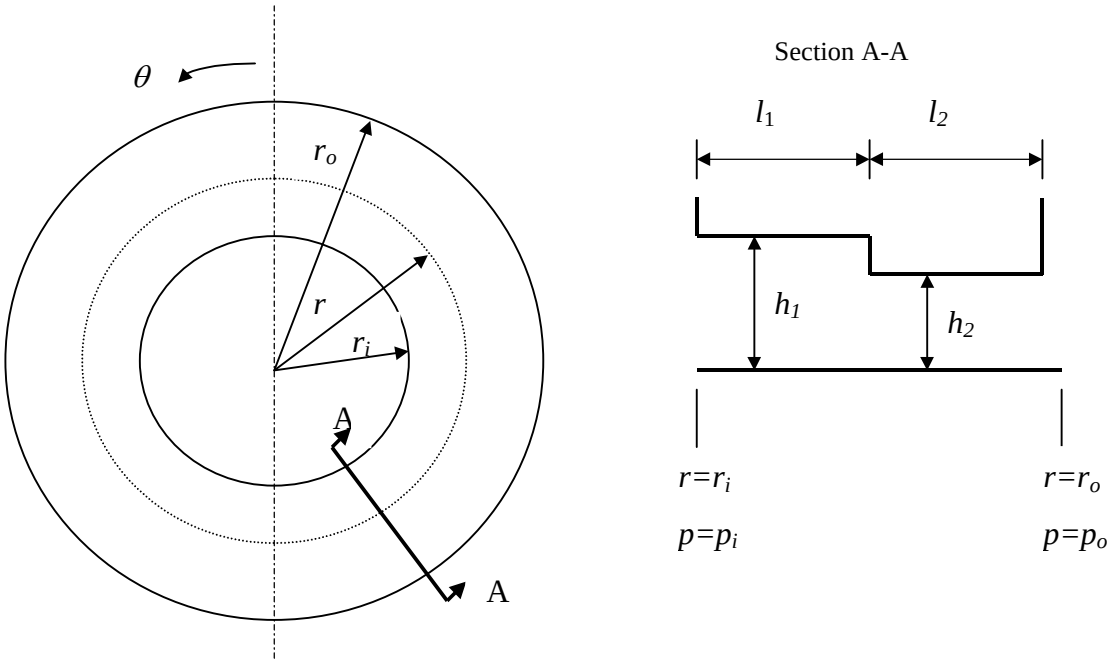

Figure 2. Schematic view of a flat mechanical face seal with outer pressure dam.

The inner, groove-ridge boundary, and outer radii are given by r_i, r_s, and r_o, respectively. The pressure dam extent is represented by l_2 and the seal extent by l_1. The seal length is $l = l_1 + l_2$. The fluid film thicknesses at the dam and at the seal are expressed by h_2 and h_1, respectively. Generally the stepped face is rotating, while the flat face is non-rotating.

The lubricant flow in the face seal is described by the Reynolds equation for an isothermal, isoviscous, ideal gas (Zirkelback and San Andrés,1999)

$$\frac{1}{r}\frac{\partial}{\partial\theta}\left(\frac{ph^3}{12\mu}\frac{1}{r}\frac{\partial p}{\partial\theta}\right)+\frac{1}{r}\frac{\partial}{\partial r}\left(r\frac{ph^3}{12\mu}\frac{\partial p}{\partial r}\right)=\frac{\Omega r}{2}\frac{\partial}{\partial\theta}(ph)+\frac{\partial}{\partial t}(ph) \tag{1}$$

where p describes the pressure field over the seal, h is the fluid film thickness, μ is the fluid viscosity, and Ω is the rotational speed of the seal. The boundary conditions for the system are given by $p(r_i)=p_i$ and $p(r_o)=p_o$. The pressures p_i and p_o are the inner and outer pressures acting on the inner and outer seal radius, respectively.

Due to the axisymmetric nature of the gas flow, the pressure field is independent of the circumferential coordinate θ. Thus, equation (1) simplifies to the following form

$$\frac{1}{r}\frac{\partial}{\partial r}\left(r\frac{ph^3}{12\mu}\frac{\partial p}{\partial r}\right)=\frac{\partial}{\partial t}(ph) \quad . \tag{2}$$

A dimensionless form of equation (2) is expressed as

$$\frac{1}{R}\frac{\partial}{\partial R}\left(RH^3P\frac{\partial P}{\partial R}\right)=\sigma\frac{\partial}{\partial \tau}(PH) \tag{3}$$

where the dimensionless variables are given by $R=\frac{r}{r_o}$, $P=\frac{p}{p_a}$, $H=\frac{h}{h_{\min}}$, $\tau=t\omega$, and $\sigma=\frac{12\mu\omega}{p_a}\left(\frac{r_o}{h_2}\right)^2$. In these variables, ω is the axial excitation frequency, p_a is the ambient pressure, and h_{min} is the minimum value of thickness. σ is the frequency or squeeze number.

Seal back springs are generally used to close the gap between the mating plates in order to restrict the fluid passage. These back springs are used to compensate the hydrodynamic and hydrostatic action of the process fluid within the gap, which tends to separate the seal mating plates.

3. PERTURBATION ANALYSIS

A perturbation procedure is applied on Eq. (3) to render the zero-th and first-order lubrication equations. The rotating face seal is usually subjected to small axial perturbations from an equilibrium position. The effect of these small axial motions is to cause small perturbations in the pressure field. The expressions for the dimensionless perturbed thickness and pressure field generated by dimensionless axial perturbations ΔZ are given in the following form.

$$H(R,\tau)=H_0(R)+\Delta Z.e^{i\tau} \tag{4}$$

$$P(R,\tau)=P_0(R)+P_1\Delta Z.e^{i\tau} \quad , \quad i=\sqrt{-1}\,. \tag{5}$$

where P_0 and P_1 represent the zero-th and first order pressure fields, respectively. H_0 is the film thickness at equilibrium position. Eq. (4) and Eq. (5) are substituted into Eq. (3) to render the zero-th and first order lubrication equations,

$$\frac{1}{R}\frac{\partial}{\partial R}\left(RH_0^3P_0\frac{\partial P_0}{\partial R}\right)=0 \tag{6}$$

$$\frac{1}{R}\frac{\partial}{\partial R}\left(RH_0^3\frac{\partial(P_0P_1)}{\partial R}+3RH_0^2P_0\frac{\partial P_0}{\partial R}\right)=i\sigma(P_0+H_0P_1) \tag{7}$$

Obtaining a closed-form solution for Eq. (6) is straightforward, however the complex coefficient equation represented by Eq. (7) requires approximate solution methods. The zero-th order pressure field can be integrated over the seal domain to render the seal dimensionless opening force *Fz*. This force represents the resultant of the hydrodynamic and hydrostatic actions of the gas thin film between the seal plates.

$$Fz=\int_{R_i}^{R_o}(P_0-1)2\pi R.dR \tag{8}$$

The complex first-order pressure field will render the dimensionless stiffness *Kzz* and damping *Czz* force coefficients for the seal. The fluid resistance to any axial relative displacement between the seal plates can be represented by the stiffness coefficient. The damping coefficient can be considered the flow resistance to any axial relative speed variation between the seal mating plates.

$$Kzz+i\sigma Czz=\int_{R_i}^{R_o}2\pi RP_1.dR \tag{9}$$

4. FINITE ELEMENT MODELING

The gas flow domain is modeled by using two-node linear finite elements of length L_e. A direct Galerkin weighted residual method is employed to render the element zero-th and first order lubrication equations. The zero-th and first order pressure fields depend only on the radial coordinate R.

The zero-th order lubrication for a finite element e is written as

$$K^e_{ji} P^e_i = q^e_j \quad , (i,j=1,2) \tag{10}$$

where

$$K^e_{ji} = \int_0^{L_e} RH_e^3 P_o^e \frac{d\psi^e_i}{ds}\frac{d\psi^e_j}{ds} ds \tag{11}$$

$$q^e_j = \left[R\psi^e_j m_e\right]_{s=0} - \left[R\psi^e_j m_e\right]_{s=L_e} \tag{12}$$

P^e_o is the known value of pressure prior to the computation. The dimensionless flow rate is represented by $m_e = H_e^3 P_e \frac{dP_e}{dR}$. The dimensionless flux balance over an element e is given by q^e_j. $K_{ji}{}^e$ represents the zero-th order fluidity matrix coefficients. The system of finite element equations (Eq. (10)) renders the zero-th order pressure distribution over the seal domain. An iterative procedure based on successive approximations, using the inner pressure p_i as initial guess, is used to compute the pressure field over the seal domain.

The first order finite element system of equations is obtained by using the same Galerkin procedure used in the derivation of the zero-th order equation. The first order lubrication equation for an element e is given by

$$K^e_{1\,ji} P^e_{1\,i} = q^e_{1\,j} + f^e_{1\,j} \quad , (i,j=1,2) \tag{13}$$

where

$$K^e_{1\,ji} = \int_0^{L_e} \left(RH_e^3 P_e \frac{d\psi^e_j}{ds}\frac{d\psi^e_i}{ds} + RH_e^3 \frac{dP_e}{ds}\frac{d\psi^e_j}{ds}\psi^e_i + iR\sigma H_e \psi^e_i \psi^e_j \right) ds \tag{14}$$

$$q^e_{1\,j} = \left[R\psi^e_j m^e_1\right]_{s=0} - \left[R\psi^e_j m^e_1\right]_{s=L_e} \tag{15}$$

$$f^e_{1\,j} = -\int_0^{L_e} iR\sigma P_e \psi^e_j ds - \int_0^{L_e} 3RH_e^2 P_e \frac{dP_e}{dR}\frac{d\psi^e_j}{ds} ds \tag{16}$$

P_e is the zero-th order pressure given by Eq. (10). $K^e_{1\,ji}$ represents the complex first-order fluidity matrix coefficients, $q^e_{1\,j}$ is the first-order flux balance over element e, and $f^e_{1\,j}$ represents a complex right-hand side vector. The first-order dimensionless flow rate is given by $m^e_1 = \left(H_e^3 P_e \frac{dP^e_1}{dR} + H_e^3 \frac{dP_e}{dR} P^e_1 + 3H_e^2 P_e \frac{dP_e}{dR} \right)$.

5. MESH SENSITIVITY TESTS AND VALIDATION

Firstly, the zero-th order finite element (FEM) solution for gas lubricated step face seals is compared with the analytical steady-state solution derived for Eq. (3). The steady-state form of Eq. (3) is given by Eq. (6). The computation of the analytical zero-th order pressure field from Eq. (6) is straightforward. On the other hand, it is not so simple to obtain a closed-form solution for the first-order lubrication equation given by Eq. (7).

Figure 3 depicts the comparative results for dimensionless zero-th order pressure for an example of gas step face seal with inner pressure dam. The baseline parameters used in this validation example are $P_o/P_i=5$; $H_1/H_2=0.5$; $R_i=0.8$; $R_s=0.9$; $R_o=1$. The solid line represents the finite element solution obtained with 50 elements, while the symbols represent the analytical solution. It is shown on Figure 3 that the FEM predictions match very well the analytical results.

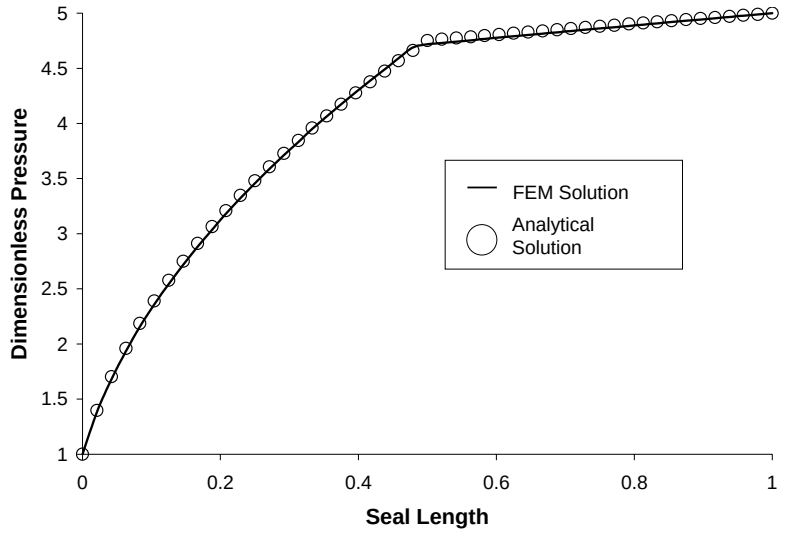

Figure 3. Dimensionless radial pressure computed by the FEM procedure in comparison with analytical results.

A preliminary evaluation of the dependence of the FEM seal opening force predictions to the mesh size is shown on Fig 4. The seal parameters employed in this study of mesh size dependence are $P_o/P_i=5$; $H_1/H_2=0.2$; $R_i=0.9$; $R_s=0.95$; $R_o=1$. From the results presented on Fig. 4 it can be noticed that the predictions of opening force practically do not vary for finite element meshes with more than 90 elements.

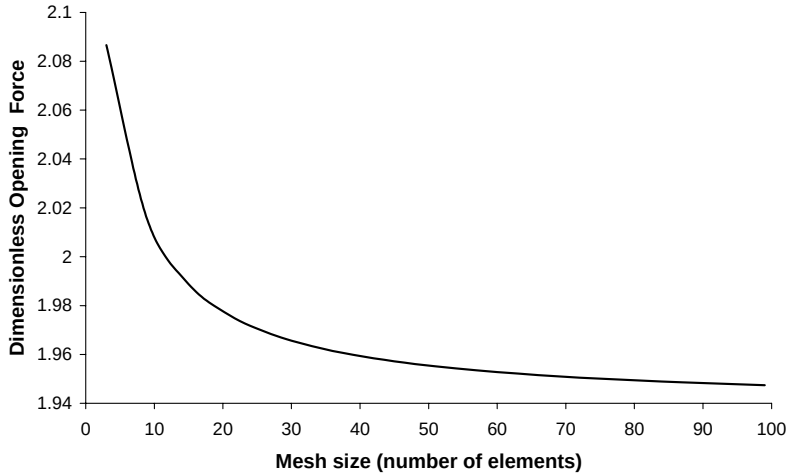

Figure 4. Mesh size sensitivity of the seal opening force computation.

6. NUMERICAL PREDICTIONS FOR GAS FACE SEAL PERFORMANCE CHARACTERISTICS

The dimensionless opening force (F_z), flow leakage rate (Q), stiffness coefficient (K_{zz}) and damping coefficient divided by the frequency number (C_{zz}/σ) are computed for several cases of gas face seals with outer and inner pressure dam. The predicted values of seal performance characteristics are shown for the following parameters: i. Seal radial width ($SRW = (R_o - R_i)/R_o$); ii. Seal dam extent ($\delta = (R_s - R_i)/(R_o - R_i)$ for inner dam seals and $\delta = (R_o - R_s)/(R_o - R_i)$ for outer dam seals); iii. Seal pressure ratio ($PR = P_o/P_i$ for inward radial flow and $PR = P_i/P_0$ for outward radial flow); iv. Seal clearance ratio ($CR = H_2/H_1$ for inner dam seals and $CR = H_1/H_2$ for outer dam seals).

For convenience, this section is divided into two items: 6.1. Comparative analysis of outer and inner dam face seals; 6.2. Seal performance characteristics. Firstly, the squeeze effects and the radial pressure gradient effects are evaluated for both cases of seals. The analysis of the squeeze effects intends to show how periodical axial motions are sensed by the gas film within the seal plates in both cases of inner and outer pressure dams. The analysis of the radial pressure gradient effects is planned to evaluate comparatively the performance of both seals under several operating conditions. Secondly, some steady-state and dynamic performance characteristics of seals with inner pressure dams are predicted in function of the pressure dam geometric parameters.

6.1. Comparative analysis of stepped seals with outer and inner pressure dams

A first example chosen to evaluate comparatively the performance of seals with inner and outer pressure dams consists on the analysis of the squeeze effects on the seal dynamic force coefficients. Disregarding any radial pressure drop along the seal plate, stiffness and damping coefficients are computed for plain seals (flat plates without any dam) and stepped seals (flat plates with inner and outer dams) with respect to the frequency number. In this case, the trapped gas within the seal lands must respond to periodical axial motions at different excitation frequencies. Figure 5 depicts the comparative values of dimensionless axial stiffness (K_{zz}) versus frequency number for a plain seal, a stepped seal with inner dam and a stepped seal with outer dam. The solid line represents the FEM predictions for plain seals, while the dashed lines with symbols represent the predictions for both stepped seals. The basic seal parameters are $P_o/P_i=1$; $H_1/H_2=0.5$; $R_i=0.8$; $R_s=0.9$; $R_o=1$. The finite element mesh uses 100 elements. The seal axial stiffness increases as the frequency number increases, tending to level off at high values of frequency number. The gas resistance to any axial motion seems to be directly associated with the gas volume trapped within the seal lands. That is the reason for plain seals present higher stiffness than those presented by stepped seals when there is no radial pressure drop along the seal face. Stiffness coefficients of inner and outer stepped seals present very similar response to the squeeze effects.

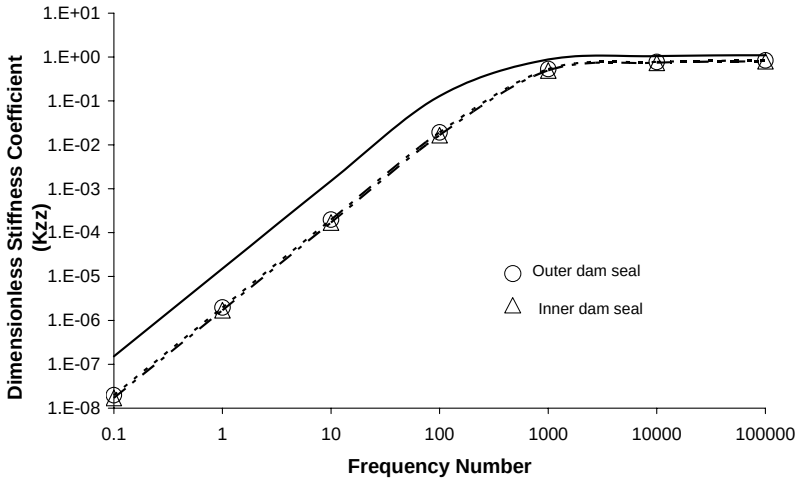

Figure 5. Comparative dimensionless stiffness coefficients due to the squeeze effects (solid line represents the plain seal predictions and dashed lines represent predictions for stepped seals).

The comparative predictions of dimensionless damping coefficients due to the squeeze effects are shown on Fig. 6. It is noticeable that the damping coefficients depict initially an increasing trend and, then, turn to a decreasing trend. Perhaps the gas compliance changes caused by high excitation frequencies may explain this damping pattern. Plain seals generally offer more resistance to axial velocity changes than stepped seals do, when the gas hydrostatic action associated with the radial pressure drop is disregarded.

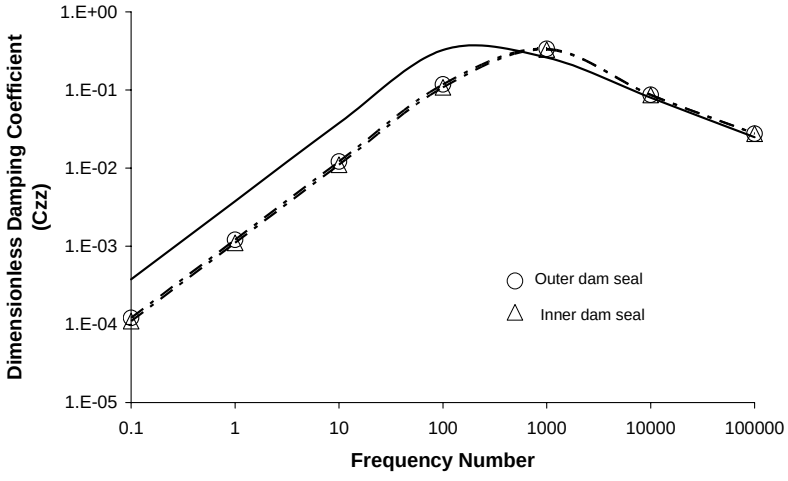

Figure 6. Comparative dimensionless damping coefficients due to the squeeze effects (solid line represents the plain seal predictions and dashed lines represent the predictions for stepped seals).

Now, a second example is designed to analyze the dynamic performance of stepped seals subjected to radial pressure ratios (hydrostatic action). The baseline parameters for this example are $P_o/P_i=5$ *or* 10; $H_1/H_2=0.5$; $R_i=0.8$; $R_o=1$; $\delta=0.1$. 100 finite elements are used to model the gas flow domain. The performance of seals with inner pressure dams are compared against the performance of seals with outer dams. Figure 7 shows the comparative values of dimensionless stiffness coefficients at two pressure ratios (*PR* = 5 and *PR* = 10). The solid lines represent the predictions for outer dam seals, while the dashed lines are associated with inner dam seals. The results show that gas seals with inner pressure dams are stiffer than gas seals with outer dams. An explanation for this fact may be that the gas volume confined by an inner dam is greater than that confined by an outer dam.

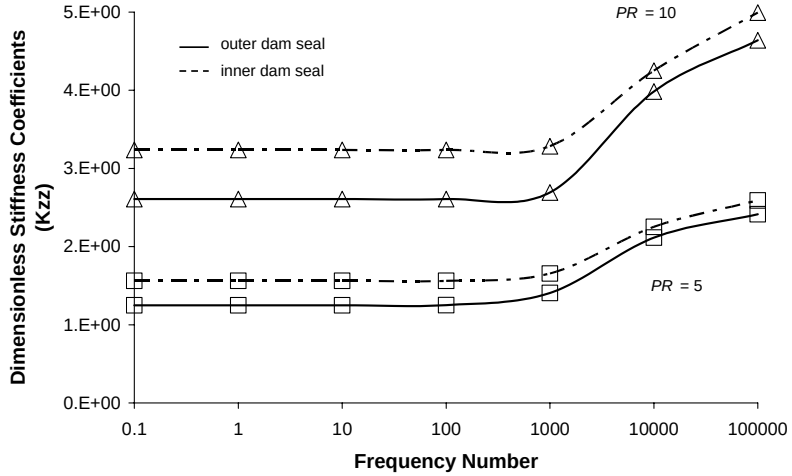

Figure 7. Comparative dimensionless stiffness coefficients for stepped seals with inner and outer pressure dams.

Figure 8 depicts the comparative values of damping coefficients predicted for stepped seals with inner and outer pressure dams. The seal parameters are the same of those used to render Fig. 7. Solid lines are associated with the damping coefficients of seals with outer dams, while the dashed lines represent the predictions for seals with inner dams. Outer dam seals provide a little more of axial damping to the system than that offered by inner dam seals.

From the computational results shown on Fig. 7 and Fig. 8, it can be stated that pressure dams introduced onto seal inner radius lead to more efficient seal designs. However, some face seals are subjected to outward radial flow, consequently demanding the use of outer seal.

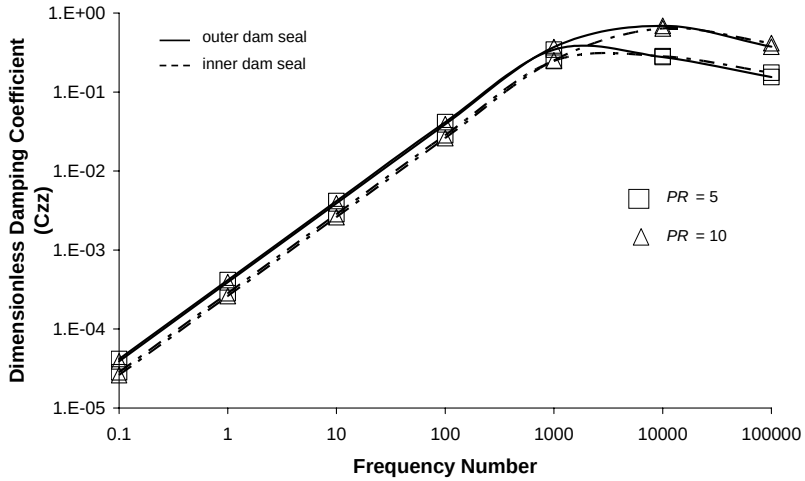

Figure 8. Comparative dimensionless damping coefficients for stepped seals with inner and outer pressure dams.

6.2. Inner dam seal performance characteristics

In this work, the stepped gas seal performance characteristics are predicted only for seals with inner pressure dam. Figure 9 depicts the variation of *Fz* and *Q* with increasing values of δ. The geometric parameters used in this analysis are $R_i=0.8$; $R_o=1$; δ *varies*. The finite element mesh employs 200 elements. Solid lines represent the predicted values obtained for *SRW*=0.1, while the dashed lines are for *SRW*=0.2. Squares indicate the values computed for

CR=2.5, while triangles are for *CR*=5. Figures 9(a) and 9(c) are computed for *PR*=5, while Figure 9(b) and 9(d) are for *PR*=10. The results show that opening force and leakage flow decrease as the seal dam extent increases. Wider sealing dams (larger *SRW*) lead to lower leakage flows and higher opening forces. Smaller clearance ratios (smaller *CR*) produce lower leakage flows mainly for small dam extent.

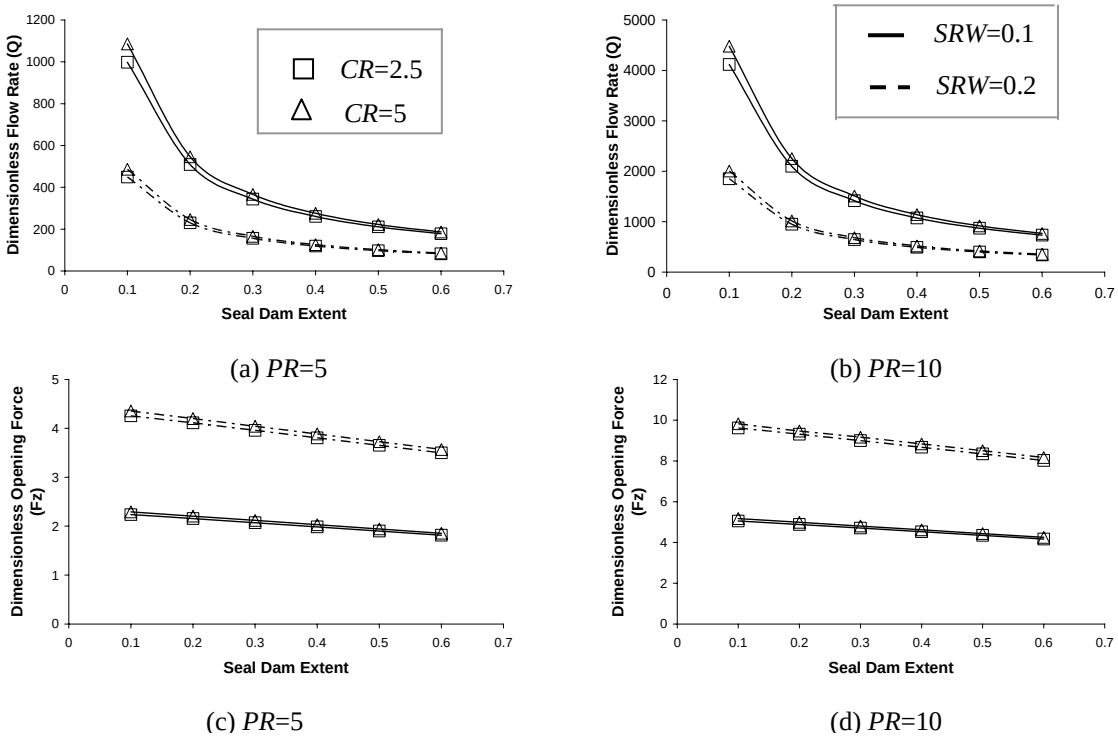

(a) *PR*=5 (b) *PR*=10

(c) *PR*=5 (d) *PR*=10

Figure 9**.** Dimensionless opening force and flow leakage rate versus the seal dam extent.

Figure 10 shows the dimensionless frequency-dependent stiffness coefficient (*Kzz*) versus the seal dam extent determined at three values of frequency number (low, medium and high). Solid lines represent the values of *Kzz* computed for *SRW*=0.2, while the dashed lines are associated with *SRW*=0.1. Squares indicate the values computed at σ=10, triangles are for σ=100, and circles are for σ=1000. *Kzz* generally increases as σ increases. Narrower seals (smaller *SRW*) lead to more flexible seal designs. In narrow seals (*SRW* = 0.1), the stiffness coefficients present a decreasing trend as the seal dam extent increases, for any frequency number. Wider seals (*SRW* = 0.2) present a response more sensitive to the frequency number. At medium and low values of squeeze number, stiffness coefficients depict a decreasing trend in wide seals, following the same pattern observed in narrow seals. On the other hand, at high frequency numbers, the stiffness coefficients of wide seals initially decrease and, then, tend to increase as the dam extent increases. At high axial excitation frequency, compressible fluids can experience significant compliance changes (Zirkelback and San Andrés, 1999) that could explain the peculiar pattern of the stiffness coefficients in wide seals.

Curves of the dimensionless damping coefficient (Czz/σ) versus the seal dam extent for different values of seal width and frequency number are depicted in Figure 11. Solid lines represent the dimensionless damping coefficients predicted by the FEM procedure for wide seals (*SRW*=0.2), while the dotted lines are associated with the predictions for narrow seals (*SRW*=0.1). As expected, (Czz/σ) increases as either the seal width or the sealing dam extent increases. The seal damping coefficient presents a decreasing trend for increasing values of frequency number.

7. CONCLUSIONS

A finite element procedure is specially devised to analyze the behavior of gas lubricated flat mechanical face seals with pressure dams. The first important conclusion drawn from the results presented in this paper is that seals with inner pressure dams can perform slightly better than seals with outer pressure dams. Moreover, seal opening force, flow leakage rate and dynamic force coefficients are computed in relation to some seal parameters, such as dam extent, clearance ratio and seal width. At high frequency numbers, the finite element predictions for dynamic force coefficients show that the fluid compressibility effects can affect considerably the seal dynamic behavior. The analysis also shows that the larger values of seal opening force, flow leakage rate and stiffness coefficient are obtained for smaller dam extents, at low and medium frequency numbers. Furthermore, the seal damping coefficients increase as the dam extent increases.

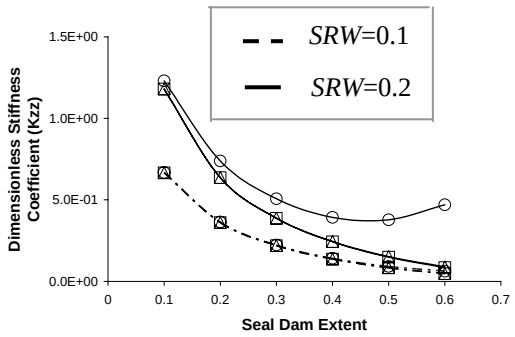

(a) *CR*=2.5 and *PR*=5

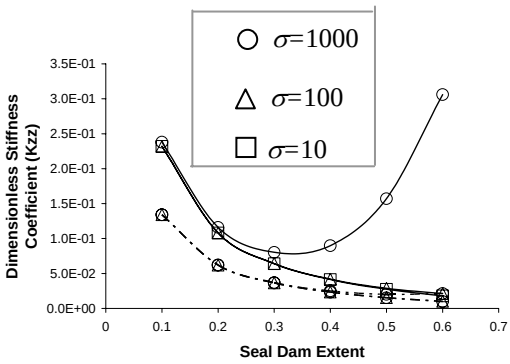

(b) *CR*=5 and *PR*=5

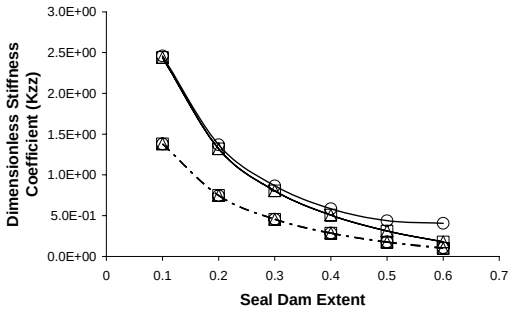

(c) *CR*=2.5 and *PR*=10

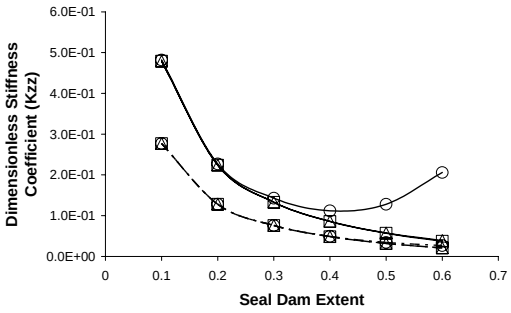

(d) *CR*=5 and *PR*=10

Figure 10. Dimensionless stiffness coefficients versus the seal dam extent at different values of frequency number.

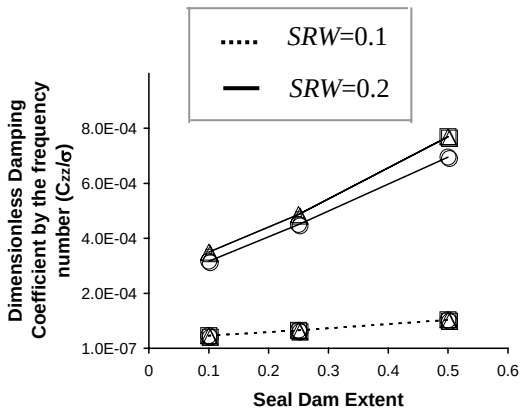

(a) *CR*=2.5 and *PR*=5

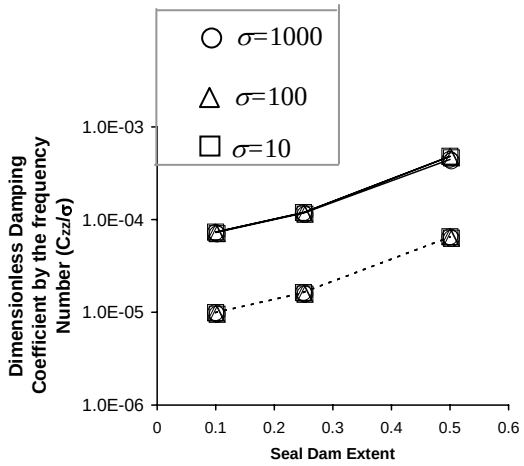

(b) *CR*=5 and *PR*=5

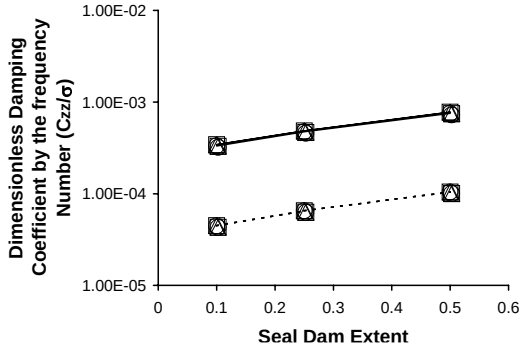

(c) *CR*=2.5 and *PR*=10

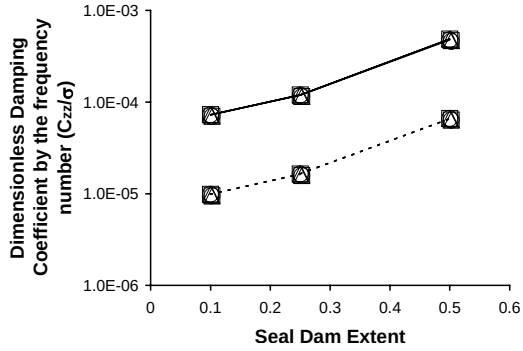

(d) *CR*=5 and *PR*=10

Figure 11. Dimensionless damping coefficient by the frequency number (Czz/σ) versus the seal dam extent at different values of frequency number.

8. REFERENCES

Allaire, P.E., 1984, "Noncontacting Face Seals for Nuclear Applications – A Literature Review", STLE Lubrication Engineering, Vol. 40, n. 4, pp. 344-351.

Basu, P., 1992, "Analysis of a Radial Groove Gas Face Seal", STLE Tribology Transactions, Vol. 35, n. 1, pp. 11-20.

Burgmann Dichtungswerke GmbH & Co., 1997, "Gas Lubricated Mechanical Face Seals", First Edition, Wolfratshausen, Germany.

Dulak, J.J., 1990, "Sealing Hazardous Gas", Machine Design, March 8, pp. 1-2.

Etsion, I., Kligerman, Y. and Halperin, G., 1992, "Analytical and Experimental Investigation of Laser-Textured Mechanical Face Seals", Proceeding of the 46th STLE Annual Meeting, Montreal, Canada, pp. 142-148.

Gabriel, R.P., 1994, "Fundamentals of Spiral Groove Noncontacting Face Seals", STLE Lubrication Engineering, pp. 215-224.

Hernandez, P. and Boudet, R., 1995, "Modelling of the Behaviour of Dynamical Gas Seals: Calculation with a Finite Element Method Implicitly Assuring the Continuity of Flow", Proceedings of the Institution of Mechanical Engineers, Part J: Journal of Engineering Tribology, Vol. 209, pp.195-209.

Huebner, K.H., Thornton, E.A. and Byrom, T.G., 1995, "The Finite Element Method for Engineers", John Wiley & Sons, 3rd Ed., New York, USA.

Kowalski, C.A. and Basu, P., 1995, "Reverse Rotation Capability of Spiral-Groove Gas Face Seals", STLE Tribology Transactions, Vol. 38, n. 3, pp. 549-556.

Lebeck, A.O. and Albor, G., 1999, "Double Gas Seal with Coplanar Coaxial Rayleigh Pad Faces for Pump Sealing Applications", Proceedings of the 16th International Pump Users Symposium, Houston, USA, pp. 69-76.

Salant, R.F. and Homiller, S.J., 1992a, "The Effects of Shallow Groove Patterns on Mechanical Seal Leakage", STLE Tribology Transactions, Vol. 35, n. 1, pp. 142-148.

Salant, R.F. and Homiller, S.J., 1992b, "Stiffness and Leakage in Spiral Groove Upstream Pumping Mechanical Seals", Proceedings of the 47th STLE Annual Meeting, Philadelphia, USA, pp. 1-6.

Tournerie, B., Huitric, J., Bonneau, D. and Frene, J., 1994, "Optimisation and Performance Prediction of Grooved Face Seals for Gases and Liquids", Proceeding of the 14th International Conference on Fluid Sealing, Firenze, Italy, 6-8 April, pp. 351-365.

Wasser, J.R., 1994, "Dry Seal Technology for Rotating Equipment", STLE Lubrication Engineering, Vol. 50, n. 3, pp. 247-252.

Zirkelback, N. and San Andrés, L., 1999, "Effect of Frequency Excitation on the Force Coefficients of Spiral Groove Gas Seals", ASME Journal of Tribology, Vol. 121, n. 4, pp. 853-863.

5. RESPONSIBILITY NOTICE

The authors are the only responsible for the printed material included in this paper.